

Article

Removal of Methylene Blue from Aqueous Solution by Bone Char

Puqi Jia ^{1,2,3}, Hongwei Tan ³, Kuiren Liu ² and Wei Gao ^{3,*}

¹ College of Earth and Environmental Sciences, Lanzhou University, 222 Tianshui South Road, Lanzhou 730000, China; jpq@lzu.edu.cn

² Department of Nonferrous Metallurgy, School of Metallurgy, Northeastern University, 3 Wenhua Road, Shenyang 110819, China; liukr@smm.neu.edu.cn

³ Department of Chemical and Materials Engineering, Faculty of Engineering, The University of Auckland, Private Bag 92019, Auckland 1142, New Zealand; htan393@aucklanduni.ac.nz

* Correspondence: w.gao@auckland.ac.nz; Tel.: +64-9-923-8175

Received: 31 August 2018; Accepted: 6 October 2018; Published: 12 October 2018



Abstract: Bone char was prepared from bovine bone for the removal of methylene blue from aqueous solution. The effects of particle size, contact time, and adsorption temperature on the removal rate of methylene blue were investigated. It was found that bone char particle size had an insignificant effect. The equilibration time was found at approximately 80 min. The removal rate decreased with an increase in temperature. The intraparticle diffusion was the main rate-limiting step. The experimental data was analyzed by kinetic, isotherm, and thermodynamic equations. The results show that the pseudo-second-order kinetic model and Freundlich, Temkin, and Dubinin–Kaganer–Radushkevich isotherm models are true of the adsorption process. The spontaneous and exothermic ion-exchange adsorption process was certified by the negative values of free energy change and enthalpy change, and 13.29 kJ mol⁻¹ of adsorption energy.

Keywords: bone char; methylene blue; adsorption; ion-exchange; kinetics

1. Introduction

Methylene blue (MB) is a cationic thiazine dye, widely used as a chemical indicator, dye, biological stain, and drug [1–3]. However, unbridled emissions of methylene blue into surface and underground water will harm human beings and other creatures because of its toxicity to neural tissue, reproductive system, and skin [4]. Therefore, the removal of methylene blue from effluent is important for environmental and human health.

In recent years, photocatalysis has been considered as an effective method for the oxidization of methylene blue into nontoxic products [5]. With large numbers of surface active sites, nano-sized photocatalysts have been extensively studied [6]. However, the suspension composed by nano-sized photocatalysts and methylene blue solution can block light penetration, reducing the photocatalytic efficiency. In addition, nanoparticles are difficult to reclaim, so the secondary contamination may hinder their large-scale industrial application. To solve these problems, millimeter-sized porous materials such as activated carbon [7], diatomite ball [8], vermiculite [9], and molecular sieve 5A [10] have been developed to support nano-sized photocatalysts. Moreover, the application of nanofiltration membranes [11,12] may be a potential solution for the separation of nano-sized photocatalysts from the solution.

A good catalyst support has to possess the advantages of large specific surface area, fast and strong adsorption to the pollutant, and reversible adsorptivity in room temperature to promote photocatalysis. In the list of global greenhouse gas emission contributors, agriculture ranked the second

highest, so more attention must be allocated to the utilization of agricultural waste to form sustainable solutions [13]. As one of the biggest wastes in livestock products, animal bone has to be recycled and utilized to meet the requirements of sustainable development. Meanwhile, the technological solutions to recycle waste must be conducive to sustainable industrial and social development [14].

In this paper, bone char, a low-cost material with large specific surface area, was used to study its adsorption performance for methylene blue, which may be a promising support material for photocatalysts. Bone char (BC) is made from cheap bovine bone waste products with a porous hydroxyapatite structure. It has been highly regarded as a green (nontoxic), effective, and easily regenerable adsorbent to remove hormones and methylene blue dye [15–18]. The performance of adsorbents and separation materials could be fine-tuned with various treatments such as pyrolysis treatment [19] and solvent treatment [20]. These two solutions have also been studied in our previous report [15].

The effects of bone char size, contact time, and adsorption temperature on the removal rate of methylene blue have not been studied previously; however, these are important factors to consider in the photocatalysis process. Thus, the study of these effects is the main research purpose of this work. The adsorption mechanisms of bone char for methylene blue using kinetic, isotherm, and thermodynamic theories were also studied. Finally, the ion-exchange interaction mechanism between bone char and methylene blue was proposed.

2. Experimental

2.1. Preparation and Characterizations of Bone Char

Bone char was prepared from bovine bone waste products, which were sawed into pieces of 2–3 cm in length. The bone pieces were then rinsed and boiled in deionized water three times for 4 h each to remove fat and residual protein thoroughly; they were then dried in an oven at 110 °C for 12 h. These porous solids were ground into small granules, which were sieved to particle sizes of 0.25–0.50 mm, 0.50–0.80 mm, and 0.80–1.00 mm using the ASTM (American Society for Testing and Material) standard sieves. Pyrolysis was performed in a box-type muffle furnace at 400 °C for 2 h under atmospheric conditions with a heating rate of 10 °C min⁻¹. After being cooled to approximately 50 °C, the prepared samples were transported to a desiccator.

The phase purity and crystallinity of the prepared bone char were determined by XRD (Bruker, D2 PHASER, Billerica, MA, USA) using Cu K α ($\lambda = 1.5405 \text{ \AA}$) radiation. The specific surface areas of bone char samples were detected on a surface area instrument (Micromeritics, 3 FLEX, Norcross, GA, USA) using nitrogen gas as an adsorbate and calculated according to the BET (Brunauer, Emmett and Teller) model. The FT-IR spectra of bone char samples before adsorption and after desorption of methylene blue were captured by an FT-IR spectrometer (PerkinElmer, Spectrum 100, Waltham, MA, USA).

2.2. Removal of Methylene Blue by Bone Char

Methylene blue (CAS: 122965-43-9, ECP) solutions were placed in closed brown glass bottles and agitated in an incubator shaker at a speed of 150 rpm. The effects of pH, initial dye concentration, and adsorbent dosage have been investigated in our previous research [21]. In this study, the initial pH was set as 10.4 because methylene blue can be adsorbed on the bone char surface mainly by strong electrostatic attraction between negative bone char surface adsorption sites after deprotonation and positive methylene blue ions without free chloride ions when the pH value is higher than the point of zero charge ($\text{pH}_{\text{PZC}} = 8.0$) of bone char. Another reason for this initial pH is that ZnO, the photocatalyst that will be loaded on the bone char surface in later research, is not stable at $\text{pH} \leq 5$ or ≥ 11 during photocatalysis [22]. The initial dye concentration was 4.48 mg L⁻¹, and the adsorbent dosage was 4 g L⁻¹. At certain time intervals, the concentration of methylene blue solution was identified by a UV-VIS spectrometer (Perkin Elmer, Lambda 35, Waltham, MA, USA) at 664 nm. When the adsorption

process was finished, bone char samples were washed with hot deionized water several times for thermal desorption, followed by drying for the next run. The removal rate (R) and equilibrium adsorption quantity (q_e , mg g^{-1}) of methylene blue dye were obtained as follows [23]:

$$R (\%) = (c_0 - c) \times 100/c_0 \quad (1)$$

$$q_e = (c_0 - c_e)V/m \quad (2)$$

where c , c_0 , and c_e are the dye concentrations detected at the certain, initial, and equilibrium time (mg L^{-1}), respectively [17,24,25].

2.3. Kinetic and Isotherm Models

2.3.1. Pseudo-Second-Order Kinetic Model

Because the combination of negative bone char surface and positive methylene blue ions indicated the occurrence of electron transfer, the corresponding pseudo-second-order kinetic model was used in this work. It can be given as follows:

$$t/q = 1/kq_e^2 + t/q_e \quad (3)$$

where k is the pseudo-second-order adsorption rate constant ($\text{g mg}^{-1} \text{ min}$), and q and q_e are the adsorption capacity (mg g^{-1}) at t min and equilibrium, respectively.

2.3.2. Intraparticle Diffusion Model

It is possible that intraparticle diffusion is the rate-limiting step in porous adsorption systems. Weber and Morris put forward the intraparticle diffusion approach [26], and the related equation can be presented as follows [27,28]:

$$Q = x_i + k_{id}t^{0.5} \quad (4)$$

where k_{id} is the constant of intraparticle diffusion ($\text{mg g}^{-1} \text{ min}^{-0.5}$) and is obtained from the slope of the straight-line portion fitted from the respective plots. The plot of q vs. $t^{0.5}$ may be in the presence of multi-linearity [29,30], indicating no less than two rate-limiting steps occurring during the adsorption processes. x_i —the intercept of the line—is certainly proportional to the thickness of the boundary layer.

2.3.3. Adsorption Isotherm Models

The adsorption process is described by Langmuir, Freundlich, and Temkin models, respectively. These isotherm equations can be represented respectively as below [16,17]:

The Freundlich isotherm equation can be represented as a linear form:

$$\log q_e = \log k + 1/n \log c_e \quad (5)$$

where k and n represent the adsorption capacity (mg g^{-1}) and adsorption intensity, respectively. When the n value is between 2 and 10, it is thought that adsorption occurs readily. When the n value is less than 0.5, the occurrence of adsorption becomes more difficult.

The Langmuir isotherm equation is represented as follows:

$$1/q_e = 1/q_{max}bc_e + 1/q_{max} \quad (6)$$

where q_{max} stands for the maximum adsorption amount (mg g^{-1}) and b represents the adsorption equilibrium constant (L mg^{-1}).

The Temkin isotherm can be described as follows:

$$q_e = B \ln K_t + B \ln c_e \quad (7)$$

where $B = RT b^{-1}$. The units of adsorption temperature T and the universal gas constant R are K and $\text{J mol}^{-1} \text{K}^{-1}$, respectively. The binding constant K_t is representative of the maximum binding energy, and B is a constant relevant to the adsorption heat.

In adsorption studies, the Freundlich, Langmuir, and Temkin isotherms usually are used to describe monolayer adsorption and cannot tell the mechanisms and energy of adsorption; it is the Dubinin–Kaganer–Radushkevich (DKR) isotherm that can give the adsorption mechanism and energy of adsorption process, which is expressed as a linear form [4]:

$$\ln q_e = \ln q_m - \beta \varepsilon^2 \quad (8)$$

where q_e is the adsorption quantity of methylene blue on bone char (mmol g^{-1}). q_m , β , and ε are the DKR single-layer adsorption capacity (mmol g^{-1}), adsorption energy constant ($\text{mol}^2 \text{kJ}^{-2}$), and Polanyi potential (kJ mol^{-1}), respectively. ε can be represented as follows:

$$\varepsilon = RT \ln(1 + 1/c_e) / 1000 \quad (9)$$

where c_e is the concentration of methylene blue at adsorption equilibrium time (mmol L^{-1}). β and q_m can be derived from the plot of $\ln q_e$ vs. ε^2 . The adsorption energy (E , kJ mol^{-1}) can be obtained by the following equation:

$$E = (2\beta)^{-0.5} \quad (10)$$

The types of adsorption processes can be estimated by the ranges of E , and the E values of physical and ion-exchange adsorption are below 8 kJ mol^{-1} and among $8\text{--}16 \text{ kJ mol}^{-1}$, respectively [31,32].

2.4. Adsorption Thermodynamics

The thermodynamics parameters regarding the adsorption of methylene blue by bone char, e.g., Gibbs free energy change (ΔG^0 , kJ mol^{-1}), enthalpy change (ΔH^0 , kJ mol^{-1}), and entropy change (ΔS^0 , $\text{J mol}^{-1} \text{K}^{-1}$), were obtained through the following formulas [33,34]:

$$K_d = q_{e,mol} / c_{e,mol} \quad (11)$$

$$\Delta G^0 = -RT \ln K_d \quad (12)$$

$$\ln K_d = -\Delta G^0 / RT = \Delta S^0 / R - \Delta H^0 / RT \quad (13)$$

where K_d , $q_{e,mol}$, and $c_{e,mol}$ are the thermodynamic equilibrium constant, adsorptive capacity (mg mol^{-1}), and equilibrium concentration (mg L^{-1}), respectively. ΔH^0 and ΔS^0 can be calculated from the plot of $\ln K_d - 1/T$.

3. Results and Discussion

Figure 1a shows that the XRD pattern of bone char fits well with the hydroxyapatite phase. The SEM image in Figure 1b shows the accidented surface of bone char, indicating a potentially large specific surface area.

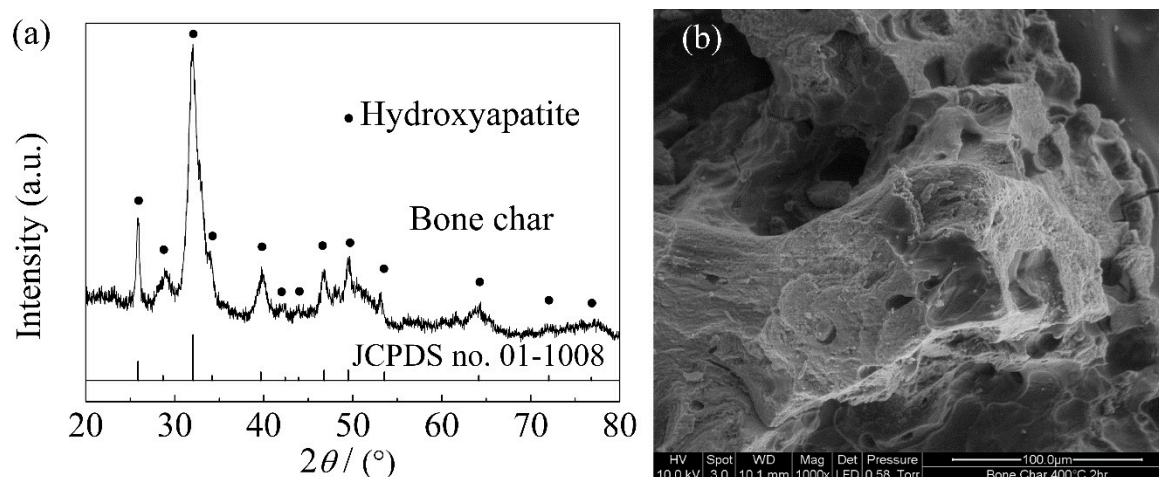


Figure 1. (a) XRD pattern of bone char and (b) SEM image [15] of bone char.

The photograph and surface areas of the bone char samples are shown in Figure 2a and Table 1, respectively. From Table 1, it can be seen that bone char with the smallest size has the biggest total and external surface area but has no pores on its surface. Further pore diameter detection shows that the pore size of bone char is between 1.7 and 75 nm, including major mesopores (2~50 nm) and a small number of pores <2 nm (micropores) or >50 nm (macropores) in diameter [15]. The chemical structure of the methylene blue molecule is shown in Figure 2b. The length of a methylene blue molecule is 13.82 Å [35] or 14.47 Å [36], and the width is approximately 9.5 Å. The length depends on the chloride ion's locations, namely whether it connects to the intermediate sulfur located in the center of the molecule or one of the two nitrogen atoms located at sides. Considering the length of the methylene blue molecule and the pore sizes of bone char, methylene blue molecules can enter into all of the pores of bone char.

As shown in Table 1, there is no association between removal rates and bone char particle size when the particle sizes are below 1.0 mm, while bone char samples with particle sizes between 0.25~0.50 and 0.50~0.80 mm have almost the same removal rate for methylene blue. The external specific surface areas of the two samples are not proportional to the removal rates. This may result from the intraparticle diffusion caused by the micropores on bone char with particle sizes of 0.50~0.80 mm. The results indicate that the adsorption process is restricted by not only the external surface but also the intraparticle diffusion. While bone char with a larger particle size of 0.80~1.00 mm has the biggest micropore specific surface area, the removal rate is slightly reduced. This is because the adsorption performance of bone char mainly depends on external diffusion. Similar results were reported in other literatures [28,37]. The errors of adsorption data listed in Table 1 were due to the existence of dynamic adsorption equilibrium.

Table 1. Effect of specific surface area on the removal rate of methylene blue by different sizes of bone char (T : 303 K, t : 24 h).

Bone Char Size (mm)	Specific Surface Area ($\text{m}^2 \text{g}^{-1}$)			Removal Rate (%)
	Total	External	Micropore	
0.25~0.50	119.21	119.21	-	45.72 ± 0.95
0.50~0.80	116.03	115.16	0.87	45.86 ± 0.57
0.80~1.00	113.13	107.73	5.40	42.35 ± 0.66

Figure 2c shows that a rather fast adsorption of methylene blue occurs on the bone char surface during the first few minutes (0~10 min), followed by two slow stages (10~40 min and 40~80 min). The second slow adsorption stage is ascribed to the decreasing diffusion path within the narrow

mesopores with possible pore blockage, further reducing diffusion [23]. In view of the length and width of the methylene blue molecule, large numbers of methylene blue dimers in water, and the micropore size of bone char, one methylene blue molecule or its dimer is enough to clog these microporous orifices. Therefore, the adsorption rate of the third stage is quite low. At last, the adsorption reaches its equilibrium at about 80 min. In this situation, the uptake rate on the surface region is much faster than the intraparticle diffusion rate in the pores [38,39]. This can be explained by the adsorption process, which follows a two-stage adsorption model governed by internal diffusion based on the Crank–Nicolson method.

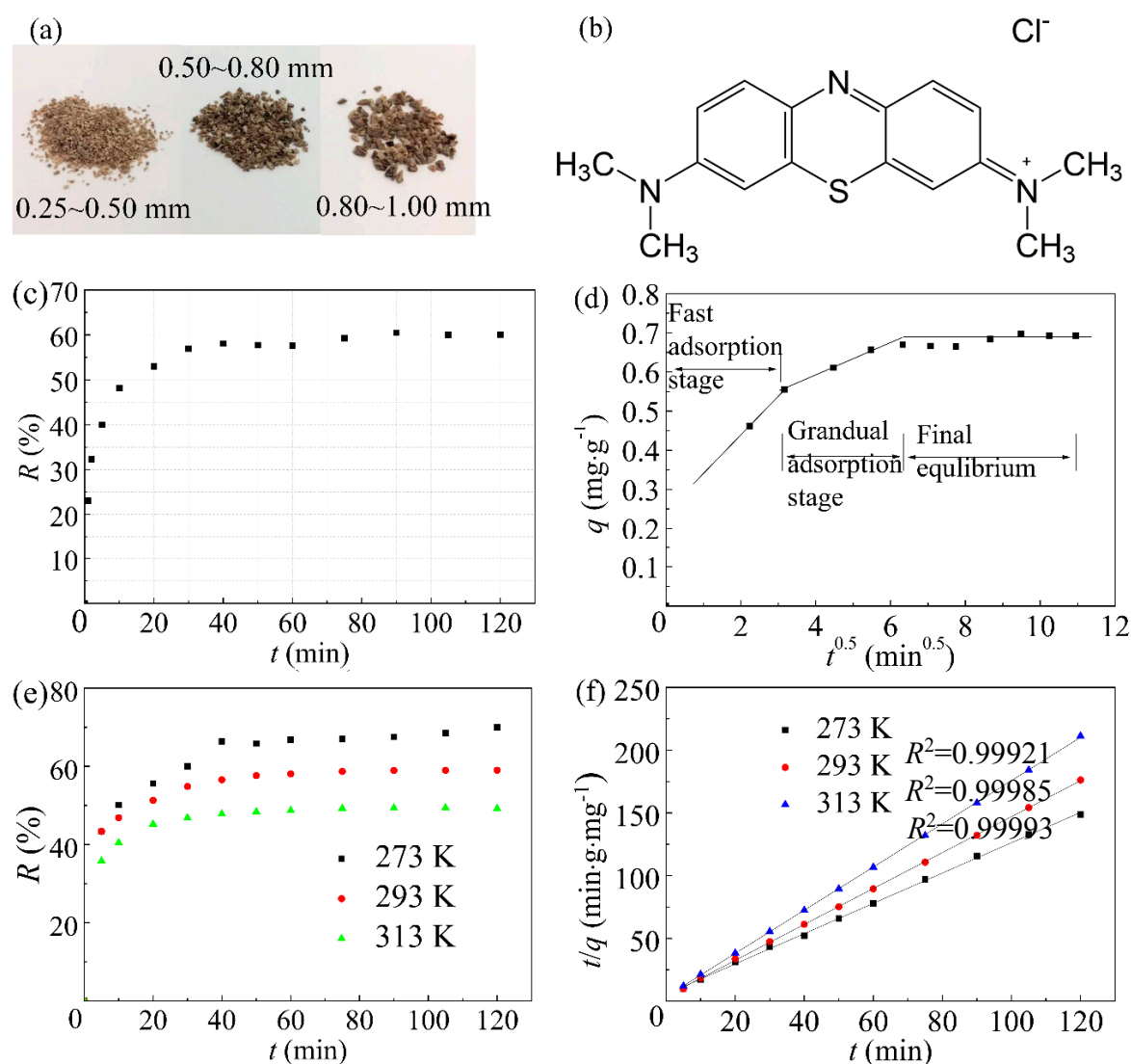


Figure 2. (a) Photograph of bone char with different sizes, (b) chemical structure of methylene blue, (c) effect of contact time on the removal rate of methylene blue (bone char particle size: 0.5–0.8 mm; T : 303 K), (d) three stages of the removal process of methylene blue by bone char represented by three continuous tend lines, (e) effect of adsorption temperature on the adsorption, and (f) pseudo-second-order kinetic model of the adsorption process (bone char particle size: 0.50–0.80 mm).

Intraparticle diffusion is expected to be the rate-limiting step during the adsorption process due to the predominant mesoporous structure of bone char. Figure 2d shows that the adsorption behavior of methylene blue onto bone char may change at different times: (a) fast adsorption of methylene blue in the first 10 min, (b) a gradual adsorption process (10–40 min) where approximately 10% of methylene blue is achieved because of the utilization of all active adsorption sites on the surface, macropores, and

mesopores of bone char, and (c) methylene blue diffuses into pores, and an adsorption equilibrium is attained. The plot of q vs. $t^{0.5}$ of the intraparticle region does not go through the original point, implying that the rate-limiting step contains not only the intraparticle diffusion but also the external diffusion in which methylene blue migrates from the solution onto the bone char surface (surface adsorption) [18,39]. The same behavior has been reported in previous papers about the removal of methylene blue onto Jordanian diatomite [28].

Figure 2e shows that the removal rate of methylene blue decreases with an increase in adsorption temperature from 273 to 313 K, revealing that the removal process is exothermic in nature [40]. It is because the highly charged ions $(MB^+)_3$ is stabilized at lower temperatures, which may enhance their ion-pairing interactions with the active adsorption sites on bone char [40]. Figure 2f shows that the experimental data fit well with the pseudo-second-order kinetic curve because of the goodness of fit R^2 highly closing to 1.

The Freundlich, Langmuir, Temkin, and DKR models were applied to the adsorption isotherm. Their R^2 values are shown in Figure 3. It turns out that the Freundlich isotherm model is the most relevant adsorption isotherm, with the highest value of R^2 (>0.99). The n value in the Freundlich model was calculated to be 5.368, which showed that this adsorption occurs readily. In addition, Temkin and DKR models also fit for the adsorption process. The three aforementioned models explain that diffusion mainly occurs on the bone char surface, and the possible mechanism and the orientations of methylene blue on the surface of bone char are the same as what occurred on the surface of diatomite [28].

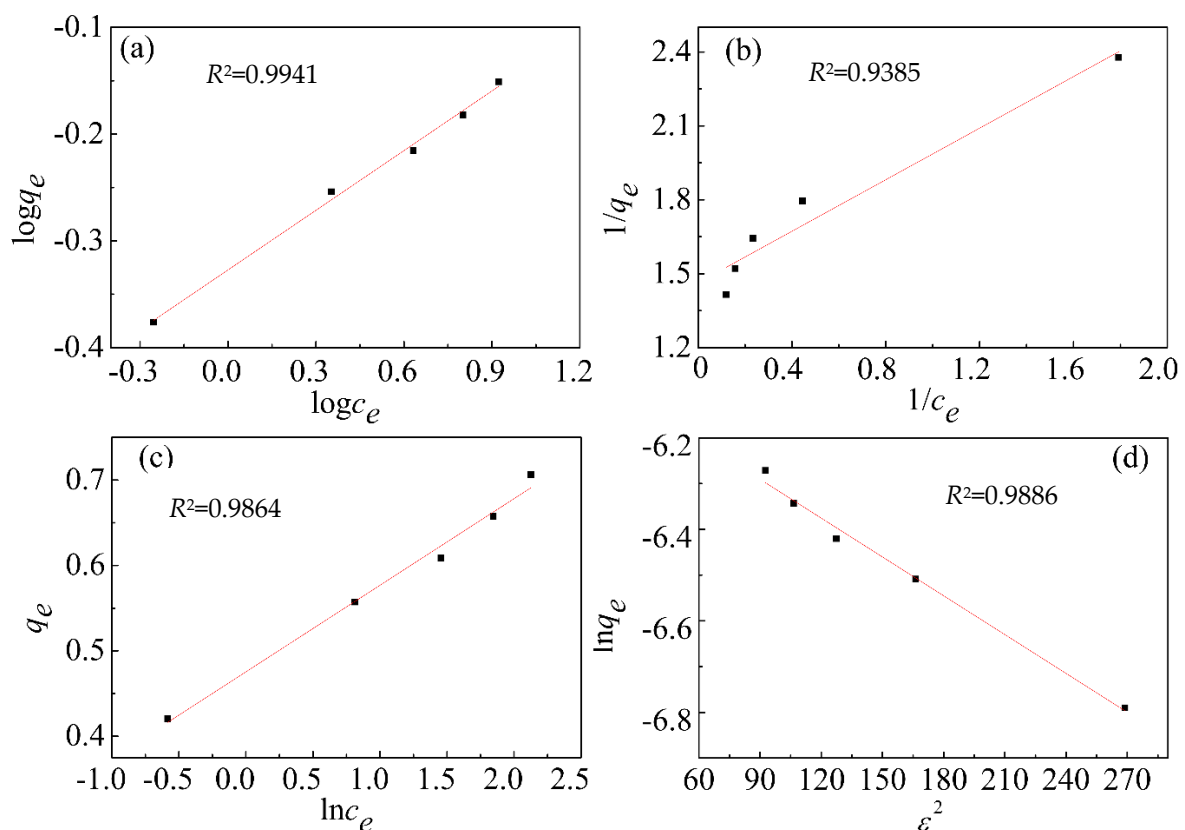


Figure 3. The adsorption data of methylene blue dye on bone char fitted with (a) Freundlich, (b) Langmuir, (c) Temkin, and (d) DKR isotherm models (particle size: 0.50–0.80 mm, T : 303 K, t : 15.5 h).

Figure 3d shows the plot of $\ln q_e$ against ϵ^2 corresponding to the removal of methylene blue by bone char. The value of E is calculated to be $13.29 \text{ kJ mol}^{-1}$, implying that the adsorption interaction between methylene blue and bone char is ion-exchange. In other words, the cationic methylene

blue takes the place of the acidic hydrogen ions of bone char during the adsorption process. Similar conclusions have been reported in other literature [41–44].

The calculated thermodynamic parameter values are shown in Table 2. The negative ΔH^0 and ΔS^0 values indicate a moderate exothermic adsorption and decreased chaos at the interface between solid and solution phases occurring during the adsorption process. The negative ΔG^0 values mean that the adsorption process is spontaneous. Furthermore, the slight increase in ΔG^0 with an increasing temperature implies that the lower temperatures result in more spontaneous adsorption. These findings were in accordance with the experimental results in Figure 2e [4,34].

Table 2. Thermodynamic parameters of the removal of methylene blue by bone char.

T (K)	K_d (L mol ⁻¹)	ΔG^0 (kJ mol ⁻¹)	ΔH^0 (kJ mol ⁻¹)	ΔS^0 (J mol ⁻¹ K ⁻¹)
273	194.58	-11.96		
293	134.36	-11.94	-13.45	-5.36
313	91.09	-11.74		

Figure 4a shows the reusability of bone char for the removal of methylene blue. The removal rates remain at 45% \pm 5% during six cycles. The standard deviation of the six data values is 3.18. After the fifth cycle, the removal rate still reaches the level of the first cycle. This result indicates that bone char has excellent adsorption stability for methylene blue and may become potential novel photocatalyst support for the removal of methylene blue.

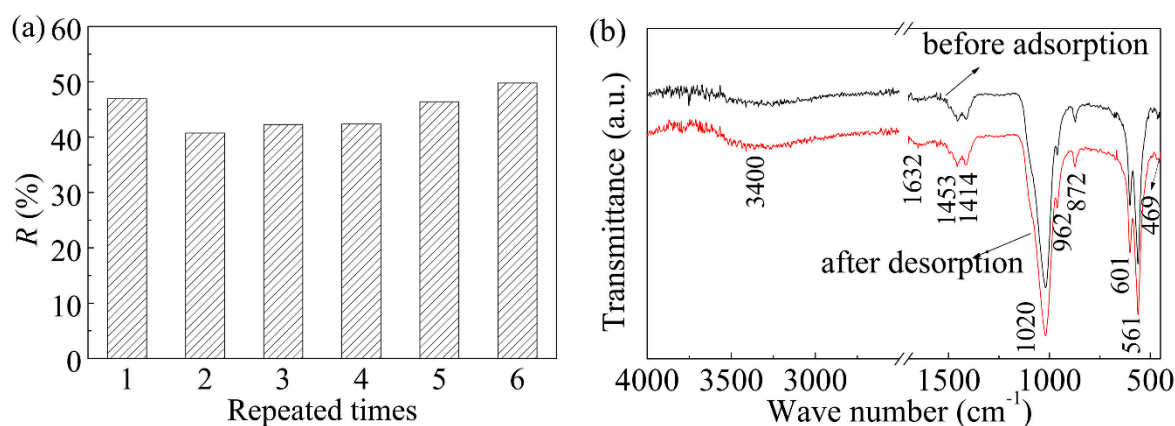


Figure 4. (a) The reusability result of bone char for the removal of methylene blue, (b) FT-IR spectra of poorly crystalline bone char sample (before adsorption and after desorption of methylene blue).

FT-IR spectra of bone char before the adsorption and after the desorption of methylene blue are shown in Figure 4b, exhibiting the characteristic bands coming from PO_4^{3-} ions at 469, 561, 601, 962, and 1020 cm^{-1} . Peaks at 1632 cm^{-1} and 3400 cm^{-1} correspond to a small amount of occluded water and O-H broad band, respectively. In addition, peaks at approximately 872, 1414, and 1453 cm^{-1} correspond to the carbonate bands of residual carbon in bone char [45]. The peak positions and intensities of the bone char samples have not changed, suggesting the reversible adsorption process.

4. Conclusions

In summary, the adsorption behaviors and mechanisms of methylene blue on bone char were studied. Results showed that the removal rate of methylene blue is highly rapid in the first ten minutes with eighty percent of adsorption capacity, which mainly relates to the external specific surface area of bone char. Then, the removal rate slows down and increasingly reaches equilibrium. It was proven that the adsorption process is internally diffusion-controlled. The removal rates of methylene blue decrease with an increase in temperature, which suggests that the adsorption process is exothermic.

The negative ΔG^0 values and the R^2 closing to 1 shown in Figure 2f demonstrate that the adsorption process is spontaneous and obeys the pseudo-second-order kinetic model. The adsorption data fit the Freundlich model very well, showing that the adsorption is single-layer and prone to occurrence. The adsorption energy value $13.29 \text{ kJ mol}^{-1}$ and reusability data of bone char states that the adsorption of methylene blue on bone char is a reversible ion-exchange process. This research suggests that bone char can be developed as a novel, effective, and regenerable adsorbent for supporting photocatalysts to adsorb methylene blue.

Author Contributions: Methodology, investigation, writing—original draft preparation, and funding acquisition, P.J.; formal analysis and data curation, H.T.; writing—review and editing, W.G.; supervision, W.G. and K.L.

Funding: This research was funded by the China Scholarship Council.

Acknowledgments: The authors appreciate the support from the China Scholarship Council, the assistance of the Advanced and Nano-Materials Research Group, and the technicians in the Department of Chemical & Materials Engineering, The University of Auckland.

Conflicts of Interest: The authors declare no conflicts of interest.

References

1. Wainwright, M.; Crossley, K. Methylene Blue—a therapeutic dye for all seasons? *J. Chemother.* **2002**, *14*, 431–443. [[CrossRef](#)] [[PubMed](#)]
2. Lin, X.; Ni, Y.; Kokot, S. An electrochemical DNA-sensor developed with the use of methylene blue as a redox indicator for the detection of DNA damage induced by endocrine-disrupting compounds. *Anal. Chim. Acta* **2015**, *867*, 29–37. [[CrossRef](#)] [[PubMed](#)]
3. Horváth, E.; Szilágyi, I.; Forró, L.; Magrez, A. Probing titanate nanowire surface acidity through methylene blue adsorption in colloidal suspension and on thin films. *J. Colloid Interface Sci.* **2014**, *416*, 190–197. [[CrossRef](#)] [[PubMed](#)]
4. Wei, W.; Yang, L.; Zhong, W.H.; Li, S.Y.; Cui, J.; Wei, Z.G. Fast removal of methylene blue from aqueous solution by adsorption onto poorly crystalline hydroxyapatite nanoparticles. *Dig. J. Nanomater. Biostruct.* **2015**, *19*, 1343–1363.
5. Rauf, M.A.; Meetani, M.A.; Khaleel, A.; Ahmed, A. Photocatalytic degradation of Methylene Blue using a mixed catalyst and product analysis by LC/MS. *Chem. Eng. J.* **2010**, *157*, 373–378. [[CrossRef](#)]
6. Houas, A.; Lachheb, H.; Ksibi, M.; Elaloui, E.; Guillard, C.; Herrmann, J.M. Photocatalytic degradation pathway of methylene blue in water. *Appl. Catal. B* **2001**, *31*, 145–157. [[CrossRef](#)]
7. Kadirova, Z.C.; Hojamberdiev, M.; Katsumata, K.; Isobe, T.; Matsushita, N.; Nakajima, A.; Sharipov, K.; Okada, K. Preparation of iron oxide-impregnated spherical granular activated carbon-carbon composite and its photocatalytic removal of methylene blue in the presence of oxalic acid. *J. Environ. Sci. Health Pt. A Toxic/Hazard. Subst. Environ. Eng.* **2014**, *49*, 763–769. [[CrossRef](#)] [[PubMed](#)]
8. Yu, X.; Xiong, L.; Ma, G.; Liang, Y.; Liu, K. Preparation and performance research of Ce-TiO₂/KL ball photocatalysts. *J. Rare Earths* **2014**, *32*, 849–854. [[CrossRef](#)]
9. Machado, L.C.R.; Torchia, C.B.; Lago, R.M. Floating photocatalysts based on TiO₂ supported on high surface area exfoliated vermiculite for water decontamination. *Catal. Commun.* **2006**, *7*, 538–541. [[CrossRef](#)]
10. Srinivas, B.; Shubhamangala, B.; Lalitha, K.; Reddy, P.A.; Kumari, V.D.; Subrahmanyam, M.; De, B.R. Photocatalytic reduction of CO₂ over Cu-TiO₂/molecular sieve 5A composite. *Photochem. Photobiol.* **2011**, *87*, 995–1001. [[CrossRef](#)] [[PubMed](#)]
11. Didaskalou, C.; Kupai, J.; Cseri, L.; Barabas, J.; Vass, E.; Holtzl, T.; Szekely, G. Membrane-grafted asymmetric organocatalyst for an integrated synthesis-separation platform. *ACS Catal.* **2018**, *8*, 7430–7438. [[CrossRef](#)]
12. Fodi, T.; Didaskalou, C.; Kupai, J.; Balogh, G.T.; Huszthy, P.; Szekely, G. Nanofiltration-enabled in situ solvent and reagent recycle for sustainable continuous-flow synthesis. *ChemSusChem* **2017**, *10*, 3435–3444. [[CrossRef](#)] [[PubMed](#)]
13. Didaskalou, C.; Buyuktiryaki, S.; Keçili, R.; Fonte, C.P.; Szekely, G. Valorisation of agricultural waste with adsorption/nanofiltration hybrid process: From materials to sustainable process design. *Green Chem.* **2017**, *19*, 3116–3125. [[CrossRef](#)]

14. Likon, M.; Cernec, F.; Svegl, F.; Saarela, J.; Zimmie, T.F. Papermill industrial waste as a sustainable source for high efficiency absorbent production. *Waste Manag.* **2011**, *31*, 1350–1356. [[CrossRef](#)] [[PubMed](#)]
15. Patel, S.; Han, J.; Qiu, W.; Gao, W. Synthesis and characterisation of mesoporous bone char obtained by pyrolysis of animal bones, for environmental application. *J. Environ. Chem. Eng.* **2015**, *3*, 2368–2377. [[CrossRef](#)]
16. Ghanizadeh, G.; Asgari, G. Adsorption kinetics and isotherm of methylene blue and its removal from aqueous solution using bone charcoal. *React. Kinet. Mech. Cat.* **2011**, *102*, 127–142. [[CrossRef](#)]
17. Rezaee, A.; Ghanizadeh, G.; Behzadiyannejad, G.; Yazdanbakhsh, A.; Siyadat, S. Adsorption of endotoxin from aqueous solution using bone char. *Bull. Environ. Contam. Toxicol.* **2009**, *82*, 732–737. [[CrossRef](#)] [[PubMed](#)]
18. Iriarte-Velasco, U.; Sierra, I.; Cepeda, E.A.; Bravo, R.; Ayastuy, J.L. Methylene blue adsorption by chemically activated waste pork bones. *Color. Technol.* **2015**, *131*, 322–332. [[CrossRef](#)]
19. Rojas-Mayorga, C.K.; Mendoza-Castillo, D.I.; Bonilla-Petriciolet, A.; Silvestre-Alberro, J. Tailoring the adsorption behavior of bone char for heavy metal removal from aqueous solution. *Adsorpt. Sci. Technol.* **2016**, *34*, 368–387. [[CrossRef](#)]
20. Razali, M.; Didaskalou, C.; Kim, J.F.; Babaei, M.; Drioli, E.; Lee, Y.M.; Szekely, G. Exploring and exploiting the effect of solvent treatment in membrane separations. *ACS Appl. Mater. Interfaces* **2017**, *9*, 11279–11289. [[CrossRef](#)] [[PubMed](#)]
21. Jia, P.Q.; Tan, H.W.; Liu, K.R.; Gao, W. Adsorption behavior of methylene blue by bone char. *Int. J. Mod. Phys. B* **2017**, *31*, 1744099. [[CrossRef](#)]
22. Han, J.; Qiu, W.; Gao, W. Potential dissolution and photo-dissolution of ZnO thin films. *J. Hazard. Mater.* **2010**, *178*, 115–122. [[CrossRef](#)] [[PubMed](#)]
23. Allen, S.; McKay, G.; Khader, K. Intraparticle diffusion of a basic dye during adsorption onto sphagnum peat. *Environ. Pollut.* **1989**, *56*, 39–50. [[CrossRef](#)]
24. Crittenden, J.C.; Trussell, R.R.; Hand, D.W.; Howe, K.J.; Tchobanoglous, G. Water quality management strategies. In *MWH's Water Treatment: Principles and Design*, 3rd ed.; John Wiley & Sons: Hoboken, NJ, USA, 2012; Volume 10, p. 184. ISBN 9780470405390.
25. Karaoğlu, M.H.; Doğan, M.; Alkan, M. Removal of cationic dyes by kaolinite. *Micropor. Mesopor. Mater.* **2009**, *122*, 20–27. [[CrossRef](#)]
26. Weber, W.J.; Morris, J.C. Kinetics of adsorption on carbon from solution. *J. Sanit. Eng. Div.* **1963**, *89*, 31–60.
27. Jain, C.; Sharma, M. Adsorption of cadmium on bed sediments of river Hindon: Adsorption models and kinetics. *Water Air Soil Pollut.* **2002**, *137*, 1–19. [[CrossRef](#)]
28. Al-Ghouti, M.A.; Khraisheh, M.A.; Ahmad, M.N.; Allen, S. Adsorption behaviour of methylene blue onto Jordanian diatomite: A kinetic study. *J. Hazard. Mater.* **2009**, *165*, 589–598. [[CrossRef](#)] [[PubMed](#)]
29. Ip, A.W.M.; Barford, J.P.; McKay, G. A comparative study on the kinetics and mechanisms of removal of Reactive Black 5 by adsorption onto activated carbons and bone char. *Chem. Eng. J.* **2010**, *157*, 434–442. [[CrossRef](#)]
30. Wu, F.C.; Tseng, R.L.; Juang, R.S. Initial behavior of intraparticle diffusion model used in the description of adsorption kinetics. *Chem. Eng. J.* **2009**, *153*, 1–8. [[CrossRef](#)]
31. Inglezakisa, V.J.; Zorpos, A.A. Heat of adsorption, adsorption energy and activation energy in adsorption. *Desalin. Water Treat.* **2002**, *39*, 149–157. [[CrossRef](#)]
32. Shen, S.; Pan, T.; Liu, X.; Yuan, L.; Zhang, Y.; Wang, J.; Guo, Z. Adsorption of Pd(II) complexes from chloride solutions obtained by leaching chlorinated spent automotive catalysts on ion exchange resin Diaion WA21J. *J. Colloid Interface Sci.* **2010**, *345*, 12–18. [[CrossRef](#)] [[PubMed](#)]
33. Chen, H.; Zhao, J.; Dai, G. Silkworm exuviae—A new non-conventional and low-cost adsorbent for removal of methylene blue from aqueous solutions. *J. Hazard. Mater.* **2011**, *186*, 1320–1327. [[CrossRef](#)] [[PubMed](#)]
34. Chu, B.; Baharin, B.; Man, Y.C.; Quek, S. Separation of vitamin E from palm fatty acid distillate using silica: I Equilibrium of batch adsorption. *J. Food Eng.* **2004**, *62*, 97–103. [[CrossRef](#)]
35. De Souza Macedo, J.; da Costa Júnior, N.B.; Almeida, L.E.; da Silva Vieira, E.F.; Cestari, A.R.; de Fátima Gimenez, I.; Villarreal Carreno, N.L.; Barreto, L.S. Kinetic and calorimetric study of the adsorption of dyes on mesoporous activated carbon prepared from coconut coir dust. *J. Colloid Interface Sci.* **2006**, *298*, 515–522. [[CrossRef](#)] [[PubMed](#)]

36. Dotto, G.L.; Santos, J.M.N.; Rodrigues, I.L.; Rosa, R.; Pavan, F.A.; Lima, E.C. Adsorption of methylene blue by ultrasonic surface modified chitin. *J. Colloid Interface Sci.* **2015**, *446*, 133–140. [[CrossRef](#)] [[PubMed](#)]
37. Muinde, V.M.; Onyari, J.M.; Wamalwa, B.; Wabomba, J.; Nthumbi, R.M. Adsorption of malachite green from aqueous solutions onto rice husks: Kinetic and equilibrium studies. *J. Environ. Prot.* **2017**, *8*, 215–230. [[CrossRef](#)]
38. Desai, N.J.; Do, D.D. Adsorption of organic solutes into activated carbons—batch studies. *Chem. Eng. Commun.* **1985**, *39*, 101–125. [[CrossRef](#)]
39. Mohan, D.; Singh, K.P. Single- and multi-component adsorption of cadmium and zinc using activated carbon derived from bagasse—An agricultural waste. *Water Res.* **2002**, *36*, 2304–2318. [[CrossRef](#)]
40. Gürses, A.; Doğar, Ç.; Yalçın, M.; Açıkyıldız, M.; Bayrak, R.; Karaca, S. The adsorption kinetics of the cationic dye, methylene blue, onto clay. *J. Hazard. Mater.* **2006**, *131*, 217–228. [[CrossRef](#)] [[PubMed](#)]
41. Kumar, K.V.; Ramamurthi, V.; Sivanesan, S. Modeling the mechanism involved during the sorption of methylene blue onto fly ash. *J. Colloid Interface Sci.* **2005**, *284*, 14–21. [[CrossRef](#)] [[PubMed](#)]
42. Uddin, M.T.; Islam, M.A.; Mahmud, S.; Rukanuzzaman, M. Adsorptive removal of methylene blue by tea waste. *J. Hazard. Mater.* **2009**, *164*, 53–60. [[CrossRef](#)] [[PubMed](#)]
43. Janos, P.; Coskun, S.; Pilarova, V.; Rejnek, J. Removal of basic (Methylene Blue) and acid (Egacid Orange) dyes from waters by sorption on chemically treated wood shavings. *Bioresour. Technol.* **2009**, *100*, 1450–1453. [[CrossRef](#)] [[PubMed](#)]
44. McKay, G.; Allen, S.J.; McConvey, I.F.; Otterburn, M.S. Transport processes in the sorption of colored ions by peat particles. *J. Colloid Interface Sci.* **1981**, *80*, 323–339. [[CrossRef](#)]
45. Zhou, W.Y.; Wang, M.; Cheung, W.L.; Guo, B.C.; Jia, D.M. Synthesis of carbonated hydroxyapatite nanospheres through nanoemulsion. *J. Mater. Sci. Mater. Med.* **2008**, *19*, 103–110. [[CrossRef](#)] [[PubMed](#)]



© 2018 by the authors. Licensee MDPI, Basel, Switzerland. This article is an open access article distributed under the terms and conditions of the Creative Commons Attribution (CC BY) license (<http://creativecommons.org/licenses/by/4.0/>).